PCCP

Accepted Manuscript

ROYAL SOCIETY OF CHEMISTRY

www.rsc.org/pccp

Journal Name

RSCPublishing

ARTICLE

Electrochemical Reduction of an $Ag_2VO_2PO_4$ Particle: Dramatic Increase of Local Electronic Conductivity

Cite this: DOI: 10.1039/xoxxoooooox

Received ooth January 2012,
Accepted ooth January 2012

DOI: 10.1039/xoxxoooooox

www.rsc.org/

Kevin C. Kirshenbaum[a], David C. Bock[b], Alexander B. Brady[c], Amy C. Marschilok[b,c,*], Kenneth J. Takeuchi[b,c,*], Esther S. Takeuchi[a,b,c,*]

Previously, we reported that electrodes containing silver vanadium phosphate ($Ag_2VO_2PO_4$) powder exhibit a 15,000 fold increase in conductivity after discharge, concurrent with the formation of silver metal. In this study, in order to disentangle the complex nature of electrodes composed of electroactive powders, an electrochemical reduction of individual particles of $Ag_2VO_2PO_4$ was conducted, to more directly probe the intrinsic materials properties of $Ag_2VO_2PO_4$. Specifically, individual particle conductivity data from a nanoprobe system combined with SEM and optical imaging results revealed that the depth of discharge within an $Ag_2VO_2PO_4$ particle is closely linked to the conductivity increase. Notably, the formation of silver metal may affect both inter- and intraparticle conductivity of the $Ag_2VO_2PO_4$ material.

Introduction

Electrode materials based on vanadium have been of significant interest for electrochemical energy storage due to possible multiple electron transfers resulting in high energy density. The variable formal oxidation states (II–V) of vanadium cations lead to a rich electrochemistry.[1, 2] An example of a vanadium material that has demonstrated long term commercial battery success is the vanadium bronze, silver vanadium oxide, $Ag_2V_4O_{11}$, which is the predominant battery cathode material in batteries powering implantable cardiac defibrillators.[3-6]

Phosphate based materials have also attracted significant attention due to their chemical and thermal stability.[7] Notably, the inherently low conductivity of phosphates must be addressed in order to facilitate their use in high power applications.

We hypothesized that bimetallic phosphate materials could address the low electrical conductivity via the in-situ formation of electrically conducting metal particles upon reduction of one of the metal ions in the bimetallic compound. Thus, we identified silver vanadium phosphorous oxides, $Ag_wV_xP_yO_z$, as a material family for next generation batteries, based on the desire to obtain the chemical stability observed in other phosphate cathode materials[8], achieve multiple electron transfer inherent in vanadium based materials and through the use of bimetallic designs, provide the opportunity for the in-situ generation of a conductive silver matrix.[9, 10] The stoichiometry of the material family can be tuned to various Ag/V ratios, and the materials $Ag_2VO_2PO_4$ [9, 11-14] $Ag_{0.49}VOPO_4{\cdot}1.9H_2O$[10, 15], $Ag_{3.2}VP_{1.5}O_8$[16] and $Ag_2VP_2O_8$[17] have all been successfully prepared for electrochemical evaluation.

In the case of $Ag_2VO_2PO_4$, clear trends in the conductivity and impedance on a battery electrode level linked to the level of discharge.[12] Notably, initial discharge demonstrated a profound impact on Li/$Ag_2VO_2PO_4$ cells with a 15,000 fold decrease in impedance.[14] The decrease in impedance was concurrent with the formation of metallic Ag^0 nanoparticles as observed by ex-situ XRD and ex-situ SEM. The formation of silver metal in the cathode was confirmed at the cell level by an in-situ energy dispersive x-ray diffraction method where the location of the silver formation within the cathode could be determined.[18] Direct measurement of cathode conductivity by the four point probe technique confirmed increased conductivity at the initial stages of reduction.[12] X-ray absorption spectroscopy has been employed to obtain a detailed understanding of the geometric and electronic changes in the material upon discharge.[13] Further, $Ag_2VO_2PO_4$ is less soluble in electrolyte compared to the benchmark ICD battery cathode $Ag_2V_4O_{11}$, for which cathode solubility is a major life limiting mechanism.[19-21]

Other members of the $Ag_wV_xP_yO_z$ family, $Ag_{0.49}VOPO_4{\cdot}1.9H_2O$, $Ag_{3.2}VP_{1.5}O_8$ and $Ag_2VP_2O_8$, also exhibit the formation of an in situ conductive Ag network upon discharge.[10, 15-17] $Ag_{0.49}VOPO_4{\cdot}1.9H_2O$ possesses a high voltage profile, above 3.0 V for much of its capacity, as well as good pulse power capability.[10, 15] $Ag_2VP_2O_8$ electrodes have been used for investigating the mechanism by which silver

formation occurs, utilizing a using in-situ energy dispersive energy diffraction technique.[22, 23] Spatial distribution of Ag^0 formation in the electrode is dependent on the discharge rate, and the change in resistance at the electrode scale may be at least partially rationalized by the formation of a conductive network of silver metal as there is sufficient silver generated to create a conductive network.[22, 23] All of the prior studies of $Ag_wV_xP_yO_z$ involved measurements of bulk electrodes.

Only a limited number of studies on the electrochemistry of individual particles have been reported where the lithiation and delithiation of individual particles of the pure active material was conducted.[24-27] These studies provide the ability to interrogate the intrinsic properties of the active material directly without complications of other components commonly present in electrodes such as binders and conductive additives. Measuring the discharge characteristics of an individual particle in one study showed that it was possible to determine lithium ion diffusion to be the limiting factor in the discharge.[28] Another study reported the deformation and fracturing of individual particles of $LiCoO_2$ and $LiNiO_2$.[29]

Here we report the electrochemistry, conductivity, and visual changes associated with the electrochemical reduction of small individual particles of $Ag_2VO_2PO_4$. These small particles are aggregates of several crystallites, thus the function of grain boundaries within a particle were examined without complication of the variety of interactions occurring within a bulk electrode. Further, using a nanoprobe system, the resistance at different locations within an individual particle was measured and used to probe local resistance changes as a function of particle reduction.

Experimental methods

$Ag_2VO_2PO_4$ was synthesized on a 0.5 g scale using a previously reported hydrothermal method.[9] Ag_2O, V_2O_5, and H_3PO_4 in aqueous solution were heated in a Teflon lined autoclave for 96 h at 230°C. The synthesized material was collected using vacuum filtration and dried under a vacuum. Along with some smaller particles, the synthesis yields many millimeter-sized individual particles which were isolated by hand. Most often the crystals form blade-like shapes approximately 1 to 2 mm in length, 0.1 to 0.2 mm wide, and with a thickness typically between 0.05 and 0.15 mm. X-ray diffraction measurements of individual particles were obtained using a Rigaku Smartlab diffractometer using Cu Kα radiation.

Individual particles were used to fabricate working electrodes using two methods which were found to be electrochemically indistinguishable. For both methods, reproducible working electrode particles were individually selected for size and uniformity using an optical microscope in conjunction with a stage micrometer. The crystals were attached to a Pt wire using conductive Au paste which was then covered in an insoluble epoxy. As an alternate method, the crystals were attached to a steel wire using a conductive carbon paste.

The test cell was in a three-electrode configuration. The $Ag_2VO_2PO_4$ particle attached to a wire served as the working electrode. The counter and reference electrode were each lithium metal attached to a wire. The electrodes are placed in a shallow dish under an optical microscope and then submerged in a carbonate electrolyte (1 M $LiPF_6$ in propylene carbonate). The entire operation is conducted in a controlled humidity dry room. The electrodes are connected to a CH Instruments CH1140A single channel potentiostat for electrochemical testing. The capacity of the particles was estimated from the particle dimensions and ranged from 10 to 100 μAh. The particles of $Ag_2VO_2PO_4$ were discharged by applying a constant current, typically between 0.1 and 10 μA depending on the desired discharge rate.

Conductivity measurements were obtained using an Omicron Nanotechnologies nanoprobe system at the Center for Functional Nanomaterials at Brookhaven National Laboratory. Particles were laid flat on a graphite substrate and affixed using a small amount of epoxy at both ends of the particle. SEM imaging was used to adjust the placement of Pt-W STM tips. After the tips were pressed into the surface of the individual particles, conductance was measured using a Keithley model 4200 semiconductor characterization system. SEM images were taken on a JEOL 7600F field emission Scanning Electron Microscope at the Center for Functional Nanomaterials at Brookhaven National Laboratory.

Results and Discussion

Material Characterization

The diffraction patterns for individual particles were collected perpendicular to either the largest face (called "front face" in **Fig. 1**) or the second largest face (called "top face"). **Fig. 1(a)** presents the results of three such crystals, one of which was measured perpendicular to both the top and front faces and the other two only perpendicular to the largest face. In **Fig. 1(b)** the diffraction patterns for diffraction along the crystallographic axes as expected from the PDF file (PDF #97-007-3580 from the ICDD) are shown. By looking at the presence and relative intensity of the observed peaks we can determine in which direction the crystals form. For particles 1 and 3, the relative intensity of the two peaks at 2θ ~ 29 and 58 deg. shows that the largest face is parallel to the (h 0 0) reflections and therefore perpendicular to the crystallographic a-axis. Particle 2 shows 5 peaks of varying intensities that match the diffraction pattern expected for the (0 0 l) reflections and thus formed along the c-axis.

All of the particles formed in the shape of a blade, with larger faces ("front face" and "top face" in **Fig. 1c**) perpendicular to a long axis. From measurement of the diffraction patterns of the particles, we found that the long dimension of the particle was always the b-axis. The front face of the blade was always perpendicular to either the a- or c-axis, with the top face perpendicular to the remaining axis. Additionally, the particles seem to contain one majority phase,

and there are no indications of minority peaks (i.e., peaks from two crystallographic directions) in the diffraction patterns.

Electrochemical Testing

An individual particle with dimensions 1.15 x 0.15 x 0.09 mm^3 was discharged in a three electrode configuration using a constant current of 4.5 x 10^{-7} A, equivalent to a full discharge in approximately 50 hours. The voltage as a function of capacity (in mAh/g) estimated from the dimensions of the crystal was recorded while discharging. Optical images of the particle were taken periodically while discharging and selected images are presented indexed to the voltage profile. The voltage profile, **Fig. 2(a)**, shows the details of the initial region of the discharge and the voltage profile, **Fig. 2(b)**, shows the full range of the discharge. While there is some variation from particle to particle, the voltage profile shown is typical of the discharge profile collected with features that are seen universally.

The optical images provide insight into the progress of the discharge. Before discharge, the particle is completely orange colored and semi-transparent, indicating insulating behavior [30]. As discharge of the particle is initiated ('A' through 'C'), the voltage drops to below 2 V while the color remains unchanged. At point 'D', the region of the particle closest to the wire begins to turn black and the voltage recovers slightly. The voltage continues to increase as more of the particle changes to black ('E' through 'H') and reaches a local maximum at point 'H' when the crystal has turned completely black. From point 'H' to point 'K' the voltage decreases slowly, but continuously similar to what is seen in bulk electrodes [9]. Finally, between points 'K' and 'L' there is a jump in the voltage associated with the beginning of a fracture in the particle developing. This fracture continues to grow in 'M' and 'N', after which the particle fully fractures into smaller pieces. The discharge was terminated at 1.2 V as the sample had reacted 90% of its theoretical capacity. Under further discharge the particle fractured, accompanied by noise in the discharge profile.

The particle fracture at lower discharge voltage is believed to be due to stresses arising from lithium insertion as well as Ag^+ ion removal from the structure. The SEM images of Ag^0 nanoparticles in the reduced material are consistent with a discharge mechanism whereby Ag^+ ions are reduced, displaced from the crystal structure, and crystallize on the surface of the particles. The XRD pattern of discharged bulk material shows only silver metal indicating electrochemical milling and amorphization of the parent $Ag_2VO_2PO_4$ material.[14] This may relate to differences in the effective ionic radii of Li^+ and Ag^+ ions (76 pm for Li^+, and 115 pm for Ag^+ for coordination number = 6).[31]

The drop in voltage on initial discharge followed by a partial recovery associated with the color change that is presented in this figure is seen in all particles discharged at comparable rates. The color change observed in the single particle is consistent with observations of color change from yellow to black in discharged $Ag_2VO_2PO_4$ bulk electrodes. Thus, the observed color change is not unique to the large single particles and is consistent with the bulk material. It is notable that the color change occurs on the side of the particle closest to the connecting wire, as this is the region closest to the electron source. $Ag_2VO_2PO_4$ is insulating and as such it is reasonable that electron access would be the limiting factor in the discharge. In a recent publication on a related material, $Ag_2VP_2O_8$, we showed that in electrodes of pure

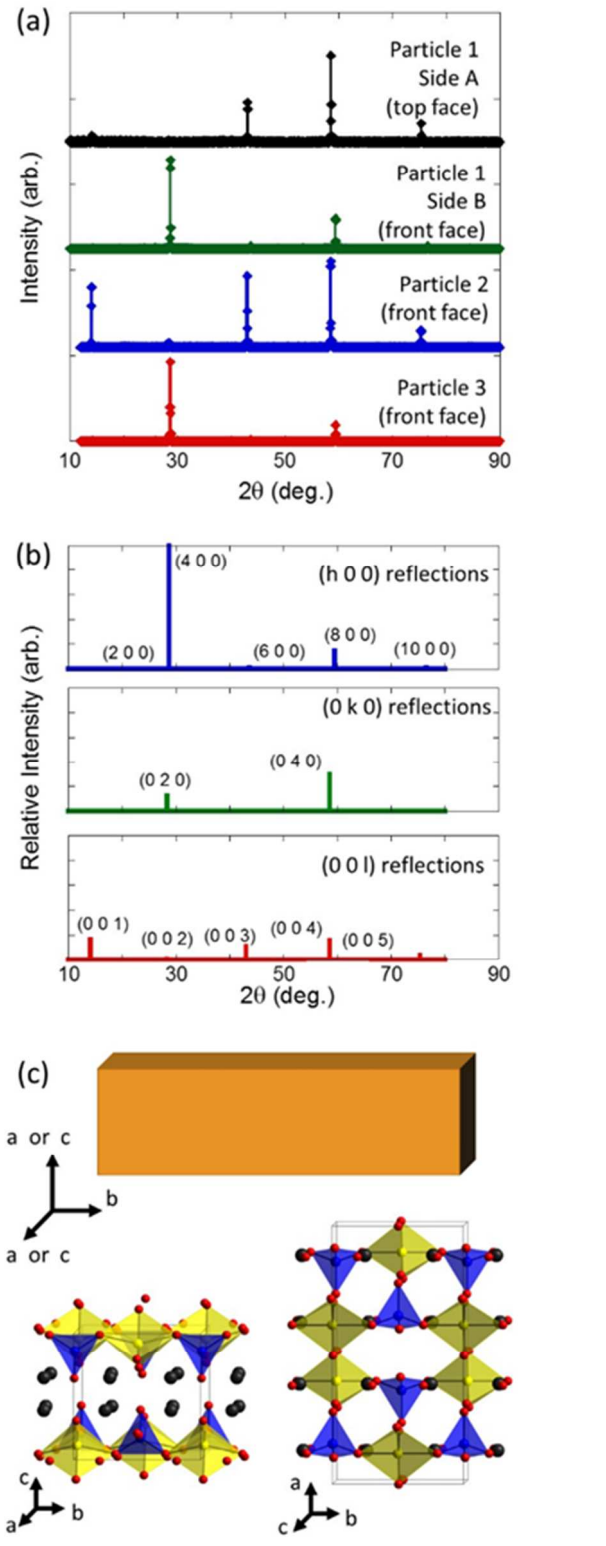

Figure 1. X-ray diffraction patterns from individual particles of $Ag_2VO_2PO_4$. **(a)** Diffraction patterns for three particles labelled 1, 2, and 3 obtained perpendicular to the largest face for all three particles and also perpendicular to the top face for particle 1. **(b)** Relative intensities of peaks along crystallographic planes expected from the powder diffraction file, obtained from ICDD (PDF #97-007-3580). **(c)** Summary of results showing possible crystal orientations with respect to particle morphology.

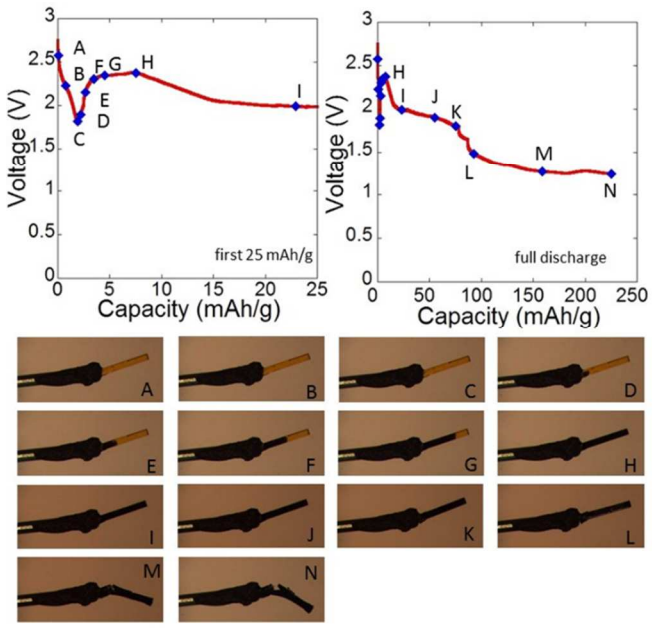

Figure 2. Constant current discharge of an individual particle of $Ag_2VO_2PO_4$. The plot in the upper left shows the details of the first 25 mAh/g of the discharge and the plot in the upper right shows the entire range of the discharge. The blue diamonds in the voltage profile correspond to the optical images taken while discharging.

active material (i.e., no conductive additives) electron access was a significant limiting factor in the discharge [22]. We propose that a similar effect is observed here where the color change is related to the enhancement of conductivity and the associated voltage increase.

The fracturing of particles seen as the discharge progresses has been observed previously in SEM images [14] and may be the cause of the increase in electrode resistance seen as the cathodes are fully reduced [12]. All of the individual particles that were fully discharged eventually fractured, however the point in the discharge at which the fracture occurred varied from sample to sample. The location of the discontinuity in the voltage (i.e., between 'K' and 'L') as well as the location within the crystal (approximately 1/3 of the way across the sample) are unique to this discharge, although similar features are seen in all fully discharged samples. The cause of these variations is most likely a function of small structural differences between the particles as well as differences in the effective discharge rate.

Scanning Electron Microscopy

Fig. 3 presents (a) an optical image of a partially discharged individual particle alongside (b)-(c) SEM micrographs of the same particle. The insulating region suffers from charging effects which causes images of the insulating region to be blurrier than those on the conducting side which we can use to distinguish the conducting and insulating regions. Similar to the results in **Fig. 4**, these images show that the boundary between conducting and insulating regions of the particles is very sharp and strongly correlated with the color change.

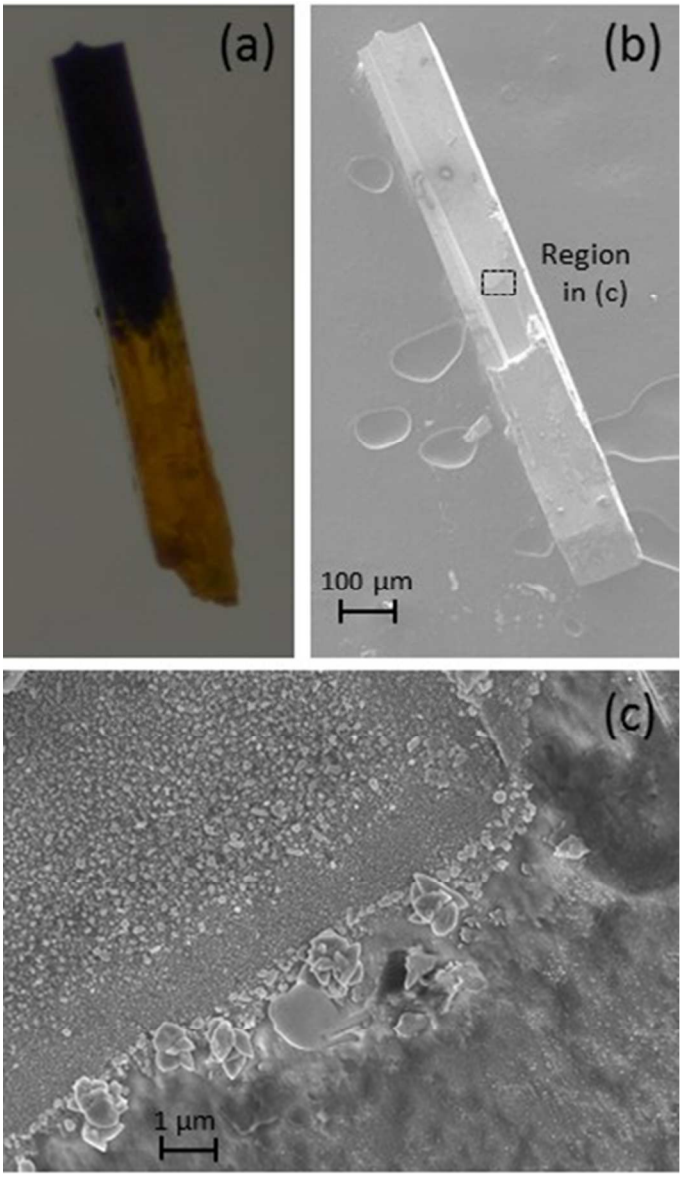

Figure 3. SEM micrographs of partially discharged particle. **(a)** optical image of individual particle showing black (conducting) and orange (insulating) regions. **(b)** SEM micrograph of entire particle. **(c)** SEM micrograph focusing on black/orange boundary.

Closer inspection of the boundary between conducting and insulating regions shows the formation of silver nanoparticles on both sides of the boundary, but with a much higher concentration and larger particle diameter in the conductive region. There is a narrow (~ 1 µm wide) region along the boundary that is electrically conductive but with a lower concentration of silver nanoparticles than areas deeper in the conductive region. We conclude that in this boundary region, the $Ag_2VO_2PO_4$ particle has begun to discharge and has become conductive, however silver metal formation is either too finely dispersed or too small to observe. As the conductivity enhancement appears to precede the formation of silver on the surface of a particle, this supports another mechanism in addition to the silver metal formation contributing to the enhancement of conductivity.

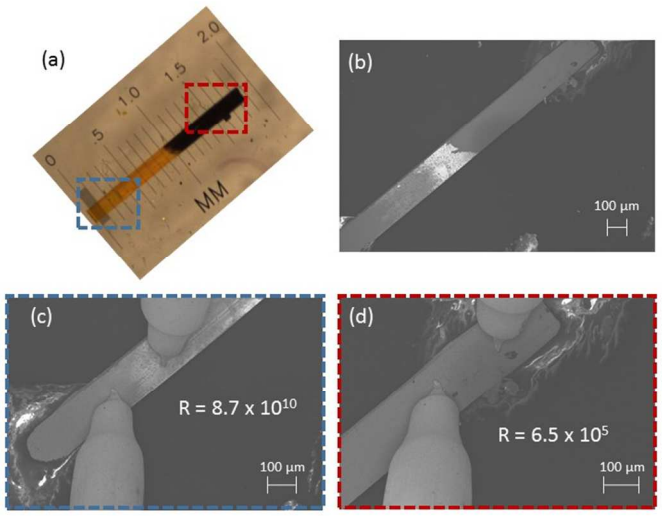

Figure 4. **(a)** Optical and **(b-d)** SEM images of a partially discharged individual particle of $Ag_2VO_2PO_4$. The two lower images show the placement of STM tips for resistance measurements of the **(c)** orange and **(d)** black regions of the particle.

Nanoprobe conductivity measurements

Individual particles at various stages of reduction were recovered and used for conductivity measurements with the Nanoprobe. A particle was discharged at a similar rate to that shown in **Fig. 2**, however the discharge was stopped at a point equivalent to 'F' in **Fig. 2**. This was done to isolate a sample with both orange and black segments such that a direct comparison of the conductivity between orange and black regions could be made. SEM micrographs alongside an optical image of the partially discharged particle indicate the two regions **Fig. 4**. The color change in the optical image corresponds to the color change seen in the SEM micrograph (**Figs. 4(a)** and **(b)**, respectively). The SEM images indicate a significant difference in conductivity between the two halves of the particle as the lighter color in the SEM image shows charging effects indicating that the region is more insulating.

To measure the resistance of the particle, two Pt-W STM tips were pressed into the surface of the particle approximately 200 µm apart. The resistance was measured within both the black and orange sections with the tip distance held constant between the two measurements. We found that the resistance of the black region (**Fig. 4(d)**) was 100,000 times lower than the resistance of the orange region (**Fig. 4(c)**), consistent with the charging observed in the SEM images.

Table 1 presents the results of resistance measurements on several individual particles discharged to different levels. Particles were discharged in one of three ways: a) partially discharged (that is, approximately half-black and half-orange colored), b) not discharged, and c) discharged to approximately 250 mAh/g (close to the theoretical capacity of 272 mAh/g). Across all samples, when resistance was measured within the

orange region of a particle the resistance was high, approximately 10^{10} to 10^{12} Ω, while the resistance measured in the black region was considerably lower, around 10^5 or 10^6 Ω. Note that the resistance measurements appear to be independent of probe distance which suggests that the current path most likely includes conduction through the substrate. For this reason the resistance values, and not resistivity, are reported here as the resistivity cannot be unambiguously calculated using simple measurements of the particle geometry.

These results show a drastic change in the electronic conduction of individual particles early in the discharge which most likely forms a large contribution to the decrease in resistance of $Ag_2VO_2PO_4$ electrodes. Moreover, this bimodal distribution associated with either the reduction of Ag^+ or V^{5+} ions may point to a fundamental change in the material. In several vanadium oxides it has been shown that chemical substitution and doping is sufficient to lower the transition temperature of a metal-insulator transition, causing the material to transition from an insulator to a metal at room temperature [32, 33]. The insertion of lithium ion into the structure appears sufficient to induce this effect.

This enhancement of conductivity explains the partial recovery of voltage as seen in 'D' though 'H' of Fig. 2. When the material is insulating, electron access is the limiting factor in the discharge and only the region of the particle closes to the wire contact is able to discharge. Locally, the particle discharges deeply until the particle begins to change color and the conductivity increases drastically. At this point there is access to regions that have not yet been discharged and the voltage recovers.

Although not investigated in this experiment, we expect that the conductivity of the discharged particles may depend upon discharge rate. A study on the related $Ag_wV_xP_yO_z$ material $Ag_2VP_2O_8$ showed that spatial distribution of Ag^0 formation is more uniform at slower discharge rates.[23] Based on this result, we expect that higher discharge rates will result in regions of higher and lower local Ag^0, and thus fewer conduction pathways in the particle.

Table 1: Resistance of individual particles of $Ag_2VO_2PO_4$ prepared in three ways: partially discharged so that the particle is approximately half black and half orange, not discharged, and fully discharged to close to the theoretical maximum

Particle details	Color of measured region	Resistance (Ω)	Distance between probes (μm)
Partially discharged particle (presented in Fig. 3)	Black	6.5×10^5	196
	Orange	8.7×10^{10}	204
Partially discharged particle	Black	2.0×10^6	72
	Orange	2.9×10^{11}	68
Non-discharged particle	Orange	1.4×10^{12}	161
Non-discharged particle	Orange	5.2×10^{11}	173
Fully discharged (to approx. 250 mAh/g)	Black	8.2×10^6	187
	Black	7.5×10^6	318
	Black	7.8×10^6	546

Conclusions

In this study we electrochemically discharged small individual particles of $Ag_2VO_2PO_4$. The particles functioned as the working electrode in a three electrode configuration, with lithium metal as counter and reference electrodes. Using this approach, we were able to disentangle the complex nature of electrodes to more directly probe intrinsic materials properties. Specifically, individual particle conductivity data from a nanoprobe system combined with SEM and optical imaging results revealed that the depth of discharge within an $Ag_2VO_2PO_4$ particle is closely linked to the conductivity increase. In previous work we asserted that as the electrodes are discharged Ag^0 metal forms and can act to decrease the interparticle resistance. This work demonstrates individual particles of $Ag_2VO_2PO_4$ show a drastic reduction (from approx. 10^{12} to 10^6 ohms) in local resistance coincident with formation of Ag^0 metal. We now propose that the early increase in conductivity of cathodes is related not only to the interparticle conductivity, but also to a significant change in the conductivity of the individual $Ag_2VO_2PO_4$ particles themselves. Notably, the formation of silver metal may affect both inter- and intraparticle conductivity of the $Ag_2VO_2PO_4$ material.

Acknowledgements

This work was supported as part of the Center for Mesoscale Transport Properties, an Energy Frontier Research Center supported by the U.S. Department of Energy, Office of Science, Basic Energy Sciences, under award #DE-SC0012673. The use of the Center for Functional Nanomaterials was supported by the U.S. Department of Energy, Office of Basic Energy Science under contract number DE-AC02-98CH10886. K. Kirshenbaum acknowledges Postdoctoral support from Brookhaven National Laboratory and the Gertrude and Maurice Goldhaber Distinguished Fellowship Program. The authors

thank Qing Zhang for assistance with scanning electron microscopy.

Notes and references

[a] Brookhaven National Laboratory, Upton, NY 11973, USA

[b] Department of Chemistry, Stony Brook University, Stony Brook, NY 11794, USA

[c] Department of Materials Science and Engineering, Stony Brook University, Stony Brook, NY 11794, USA

*Corresponding authors: (A.C.M.) amy.marschilok@stonybrook.edu; (K.J.T.) kenneth.takeuchi.1@stonybrook.edu; (E.S.T.) esther.takeuchi@stonybrook.edu.

1. E. S. Takeuchi, K. J. Takeuchi and A. C. Marschilok, in *Encyclopedia of Electrochemical Power Sources*, eds. J. Garche, C. Dyer, P. Moseley, Z. Ogumi, D. Rand and B. Scrosati, Elsevier, Amsterdam, 2009, vol. 4, pp. 100-110.
2. K. J. Takeuchi, A. C. Marschilok and E. S. Takeuchi, in *Vanadium: Chemistry, Biochemistry, Pharmacology and Practical Applications*, eds. A. S. Tracey, G. R. Willsky and E. S. Takeuchi, Taylor and Francis, New York, 2007, ch. 13.
3. K. J. Takeuchi, A. C. Marschilok, S. M. Davis, R. A. Leising and E. S. Takeuchi, *Coordination Chemistry Reviews*, 2001, 219-221, 283-310.
4. D. C. Bock, A. C. Marschilok, K. J. Takeuchi and E. S. Takeuchi, *Electrochimica Acta*, 2012, 84, 155-164.
5. K. J. Takeuchi, R. A. Leising, M. J. Palazzo, A. C. Marschilok and E. S. Takeuchi, *Journal of Power Sources*, 2003, 119-121, 973-978.
6. R. A. Leising, W. C. Thiebolt, III and E. S. Takeuchi, *Inorganic Chemistry*, 1994, 33, 5733-5740.
7. N. Iltchev, Y. K. Chen, S. Okada and J. Yamaki, *Journal of Power Sources*, 2003, 119, 749-754.
8. D. C. Bock, A. C. Marschilok, K. J. Takeuchi and E. S. Takeuchi, *Journal of Power Sources*, 2013, 231, 219-235.
9. A. C. Marschilok, K. J. Takeuchi and E. S. Takeuchi, *Electrochemical and Solid-State Letters*, 2008, 12, A5-A9.
10. Y. J. Kim, C.-Y. Lee, A. C. Marschilok, K. J. Takeuchi and E. S. Takeuchi, *Journal of Power Sources*, 2011, 196, 3325-3330.
11. Y. J. Kim, A. C. Marschilok, K. J. Takeuchi and E. S. Takeuchi, *Journal of Power Sources*, 2011, 196, 6781-6787.
12. A. C. Marschilok, E. S. Kozarsky, K. Tanzil, S. Zhu, K. J. Takeuchi and E. S. Takeuchi, *Journal of Power Sources*, 2010, 195, 6839-6846.
13. C. J. Patridge, C. Jaye, T. A. Abtew, B. Ravel, D. A. Fischer, A. C. Marschilok, P. Zhang, K. J. Takeuchi, E. S. Takeuchi and S. Banerjee, *Journal of Physical Chemistry C*, 2011, 115, 14437-14447.
14. E. S. Takeuchi, A. C. Marschilok, K. Tanzil, E. S. Kozarsky, S. Zhu and K. J. Takeuchi, *Chemistry of Materials*, 2009, 21, 4934-4939.
15. A. C. Marschilok, Y. J. Kim, K. J. Takeuchi and E. S. Takeuchi, *Journal of the Electrochemical Society*, 2012, 159, A1690-A1695.
16. Y. J. Kim, K. J. Takeuchi, A. C. Marschilok and E. S. Takeuchi, *Journal of the Electrochemical Society*, 2013, 160, A2207-A2211.
17. E. S. Takeuchi, C.-Y. Lee, P.-J. Cheng, M. C. Menard, A. C. Marschilok and K. J. Takeuchi, *Journal of Solid State Chemistry*, 2013, 200, 232-240.
18. E. S. Takeuchi, A. C. Marschilok, K. J. Takeuchi, A. Ignatov, Z. Zhong and M. Croft, *Energy and Environmental Science*, 2013, 6, 1465-1470.
19. D. C. Bock, K. J. Takeuchi, A. C. Marschilok and E. S. Takeuchi, *Dalton Transactions*, 2013, 42, 13981-13989.
20. D. C. Bock, K. J. Takeuchi, A. C. Marschilok and E. S. Takeuchi, *Physical Chemistry Chemical Physics*, 2015, 17, 2034-2042.
21. D. C. Bock, A. C. Marschilok, K. J. Takeuchi and E. S. Takeuchi, *Journal of Power Sources*, 2013, 201, 219-225.
22. K. C. Kirshenbaum, D. C. Bock, Z. Zhong, A. C. Marschilok, K. J. Takeuchi and E. S. Takeuchi, *Physical Chemistry Chemical Physics*, 2014, 16, 9138-9147.
23. K. Kirshenbaum, D. C. Bock, C.-Y. Lee, Z. Zhong, K. J. Takeuchi, A. C. Marschilok and E. S. Takeuchi, *Science*, 2015, 347, 149-154.
24. K. Dokko, N. Nakata and K. Kanamura, *Journal of Power Sources*, 2009, 189, 783-785.
25. H. Munakata, B. Takemura, T. Saito and K. Kanamura, *Journal of Power Sources*, 2012, 217, 444-448.
26. I. Uchida, H. Fujiyoshi and S. Waki, *Journal of Power Sources*, 1997, 68, 139-144.
27. A. J. J. Jebaraj and D. A. Scherson, *Accounts of Chemical Research*, 2013, 46, 1192-1205.
28. K. Dokko, M. Mohamedi, M. Umeda and I. Uchida, *Journal of the Electrochemical Society*, 2003, 150, A425-A429.
29. S. Waki, K. Dokko, T. Matsue and I. Uchida, *Denki Kagaku*, 1997, 65, 954-962.
30. N. W. Ashcroft and N. D. Mermin, *Solid state physics*, Holt, New York,, 1976.
31. R. D. Shannon, *Acta Crystallographica, Section A: Crystal Physics, Diffraction, Theoretical and General Crystallography*, 1976, A32, 751-767.
32. H. Futaki and M. Aoki, *Japanese Journal of Applied Physics*, 1969, 8, 1008-&.
33. M. Imada, A. Fujimori and Y. Tokura, *Reviews of Modern Physics*, 1998, 70, 1039-1263.